Published in Science and Technology of Materials (2007)

doi:10.1016/j.stam.2007.05.007

This is post-refreed author version

Archived in Dspace@nitr http://dspace.nitrkl.ac.in/dspace

Dielectric and Electrostrictive Properties of PMNT Near MPB

Pawan Kumar*[1] Chandra Prakash[2] and T.C. Goel[3]

[1]*Department of Physics, National Institute of Technology, Rourkela-769008, India*

[2]*DRDO Bhawan, Rajaji Marg, New Delhi-110011*

[3]*BITS Pilani-Goa Campus, Goa 403720, India*

Abstract

The dielectric constant (ε_r), dielectric loss (tanδ) and strain induced by electric field in lead magnesium niobate-lead titanate (PMN-PT/PMNT) solid solutions in the morphotropic phase boundary (MPB) region at different sintering temperatures have been studied. ε_r and tanδ increases, whereas Curie phase transition range decreases with the increase in sintering temperature. The strain levels in the range of 0.07 to 0.2% were obtained. A high saturated strain% ~0.19, a high d_{33} coefficient ~320 pm/V and a low strain hysteresis% ~3.5 in PMNT 68/32 composition sintered at 1200^{o}C indicates its suitability for actuator applications.

Keywords: Relaxor, PMNT, MPB, T_c, Strain%, Hysteresis%

Corresponding author e-mail address: pawankumar@nitrkl.ac.in, pvn77@rediffmail.com

1. Introduction

Ferroelectric ceramics are used in a variety of sensor and actuator applications. They are one of the basic building blocks of smart structures, which have been successfully used for active damping and damage detection [1]. Recent developments in the relaxor perovskite type ferroelectric materials have attracted much attention due to their greatly enhanced piezoelectric performance and strain levels compared to normal ferroelectric ceramic solid solutions. As a result, the piezoelectric, electromechanical and strain level performance of complex relaxor ferroelectrics, such as PMNT or PZNT is superior to PZT [2]. Therefore, these complex relaxor ferroelectrics are considered promising candidates for new generation of transducers and actuator materials [3].

Lead magnesium niobate (PMN) is a relaxor perovskite material, which possess a high ε_r ~20000, high electrostrictive strain at room temperature and a diffuse phase transition (~-10^{o}C) [4]. High ε_r of this material is useful for multiplayer capacitors (MLCs), pyroelectric bolometers and dynamic random memory applications (DRAM) and high electric field induced strain is useful for electrostrictive actuator applications [5]. But, its low transition temperature (~-10^{o}C) inhibits its applications in various devices. PMN forms a solid solution with lead titanate (PT), denoted as (1-x)PMN-xPT/PMNT [6]. In this system, the MPB exists between PMNT 70/30 to 65/35 compositions [7]. The compositions within this MPB region have been reported to possess ultrahigh piezoelectric response and large electric field induced strain% values with low strain hysteresis% [8-11]. The high piezoelectric and strain levels in the PMNT compositions in the MPB region are related to the co-existence of mixed structures (tetragonal and rhombhohedral) [12]. This MPB region of PMNT system is not clearly marked and different researchers have studied different compositions. Also, the development of perovskite phase and structures in the MPB region are affected by sintering temperature, which in turn affects the material properties. Hence, there is a need to study different compositions of PMNT system and the sintering temperature effects on their properties in the MPB region. In the present study, different compositions of PMNT system namely PMNT 70/30, 68/32 and 66/34 in the MPB region have been synthesized by Columbite technique. The surface morphology, dielectric and strain induced by electric field in these compositions, sintered at different temperatures, have been discussed.

2. Experimental Procedure

PMNT compositions in the MPB region were prepared by Columbite technique. The details of the processing steps have been described elsewhere [13]. Phase formation studies were performed on PW 3020 Philips type X-ray diffractometer using Cu Kα (λ=1.5405Å) radiation. The surface morphology was studied using SEM (Cambridge Stereo scan 360 scanning electron microscope) technique. ε_r and tanδ were measured at different frequencies (0.1kHz-100kHz) as a function of temperature using computer interfaced 4284A HP LCR meter. The samples were poled under corona discharge. Here, first the samples were preheated at a temperature about 100^{o}C (below T_c) and then

subjected to corona discharge by applying a voltage of 6kV for 15minutes, after which the heater was turned off while maintaining the corona voltage. Strain% versus electric field (S-E) loops were taken using SS-50 strain measurement system (Sensor Tec. Ltd., Canada), shown in Fig. 1. Electric field as high as 4.5MV/cm was applied using an amplified triangle waveform at a drive frequency of 50 Hz. All stain curves were obtained after 3rd cycle. During testing, the samples were submerged in silicon oil to prevent arcing.

3. Results and Discussions

Fig. 2 shows the evolution of X-ray diffraction patterns of PMNT 70/30, 68/32 and 66/34 compositions, each sintered at 1200^{o}C. The absence of pyrochlore phase peak (at $2\theta = 29.5^{o}$) in all these compositions confirms the formation of pure perovskite phase and the significance of using Columbite technique [14]. Sharp and distinct diffraction peaks are obtained for all the samples and the intensity of diffraction peaks increases with the increase in sintering temperature. XRD peak intensities in polycrystalline ceramics increase with the increase in grain size and density of the ceramic [15]. Therefore, the increase in peak intensities with the increase in sintering temperatures of PMNT compositions in the MPB region can be attributed to the increase in crystalline and homogeneous nature of the materials [16].

Surface morphology of PMNT 70/30, 68/32 and 66/34 compositions, each sintered at different temperatures is studied using SEM. The average grain size is calculated using the linear intercept method. For different PMNT compositions in the MPB region, grain size is found in the range of ~1 to 5μm. Porosity in the samples decreases and grain size increases with the increase in sintering temperature. As can be seen from Figs. 3.1, 3.2 and 3.3, grain size of ~1.5, 2 and 4.3μm for PMNT 70/30, whereas ~2, 3.6 and 4.3μm for PMNT 68/32 and ~3.3, 4 and 4.5μm for PMNT 66/34 compositions, each sintered at 1150, 1200 and 1250^{o}C, respectively, are obtained.

Variation of ε_r and tanδ at 1kHz frequency of PMNT 70/30, 68/32 and 66/34 compositions at different sintering temperatures has been studied. Fig. 4 shows the typical dielectric variations of PMNT 68/32 composition, sintered at 1150, 1200 and 1250^{o}C, respectively. In all the compositions, near T_c, ε_r increases with the increase in sintering temperature, whereas T_c corresponding to the peak of ε_r at 1kHz of PMNT

68/32 and 66/34 compositions is found to be decreasing. The increase in ε_r with the increase in sintering temperature can be attributed to the decrease in porosity and increase in crystallinity, homogeneity and the density of the ceramics [16]. The decrease in T_c with the increase in sintering temperature can be attributed to the increase in internal stress in the system. Here, we can consider a relationship to be present between internal stress and pores because pores can relieve internal stress, which do not constrain the grains. As shown in SEM microstructures that with the increase in sintering temperature, the porosity of the samples decreases and grain size increases, which leads to an increase in internal stress in the PMNT 68/32 and 66/34 compositions [17]. Also, the phase transformation temperature is inversely proportional to the internal stress [18]. Consequently, the decrease in T_c with the increase in sintering temperature in PMNT 68/32 and PMNT 66/34 compositions seems to be the result of increase in internal stress due to decrease in porosity [19].

Curie transition temperature (T_c) increases with the increase in PT content in PMNT system and follows the relation [20]:

$$T_c = 5x - 10, \quad \textit{where x (mole\%) is the PT content}$$

and the Curie range is calculated using the relation:

Curie range =Temperature of (½ ε_{rmax}) in paraelectric region – Temperature of (½ $\varepsilon_{rmax.}$) in the ferroelectric region.

This Curie range is found to be maximum for PMNT 70/30 composition sintered at 1150^{o}C and it decreases with the increase in sintering temperature and PT content in all the PMNT compositions in the MPB region. The dielectric broadening at the paraelectric–ferroelectric phase transition in PMNT system is due to compositional fluctuations and microscopic inhomogeneity [21-23]. Therefore, decrease in dielectric broadening with the increase in sintering temperature and increase in PT content, suggests the decrease in compositional fluctuations and microscopic inhomogeneity. The ε_r Vs. temperature plots of PMNT 68/32 and 66/34 compositions sintered at 1150, 1200 and 1250^{o}C temperatures display two major anomalies. As can be seen in Fig. 4(i), in ε_r Vs. temperature plots of PMNT 68/32 composition, sintered at different temperatures, there is a dielectric hump near 110 and 150^{o}C. The existence of two dielectric anomalies in PMNT 68/32 and 66/34 compositions is related to their MPB nature. PMNT 68/32 and

66/34 compositions belong to MPB region, therefore at room temperature there can exist mixed structures (tetragonal+rhombohedral). Near 110^{o}C, this mixed structure (tetragonal+rhombohedral) is transforming into single tetragonal structure and gives rise to a dielectric hump, whereas the second dielectric anomaly is related to the ferroelectric to paraelectric phase transition. Therefore, appearance of double dielectric anomaly in PMNT 68/32 and 66/34 compositions, sintered at different temperature, confirms their MPB nature [24]. From room temperature to 225^{o}C, tanδ is in the range of 0.008 to 0.075 for all the PMNTcompositions, sintered at different temperatures. Except in PMNT 68/32 composition, sintered at 1150^{o}C, as shown in Fig. 4(ii), tanδ increases with the increase in sintering temperature. High tanδ at room temperature in PMNT 68/32 composition, sintered at 1150^{o}C, may be attributed to the presence of intergrannular layers of a Pb-rich atmosphere, which has been successfully described by brick–wall dielectric mixing laws [25-28]. Whereas, the increase in tanδ with the increase in sintering temperature can be explained on the basis of increase in space charge conduction in the system. These space charges increases with the increase in sintering temperature due to high volatility of PbO, which can produce Pb or O site vacancies in the PMNT compositions [29]. Temperature of max. tanδ of all the MPB compositions is different than temperature of max. ε_r, which is a characteristic of relaxor ferroelectric [30] materials and Kramers-Kronig relation indicates that this can be the consequence of temperature dependent relaxation near Curie temperature [31].

Longitudinal strain induced as a function of unipolar electric field for different PMNT compositions, in the MPB region, sintered at different temperatures, is shown in Figs. 5(i), 5(ii) and 5(iii), respectively. Here, the longitudinal strain Vs. unipolar electric field measurements are taken because it is realistic to apply unipolar driving in actuator devices in order to avoid inverting the remnant polarization (P_r) or depoling of the material [32]. Strain% in the range of 0.07 to 0.2 is obtained. The strain hysteresis% is calculated using the relation [33]:

Strain hysteresis% = (hysteresis in strain% at half of the maximum electric field/ strain% at the maximum electric field) ×100

and the strain hysteresis% of ~ 6, 6.6 and 8.9 in PMNT 70/30, 3.2, 3.5 and 6.5 in PMNT 68/32 and 6.5, 3.9 and 1 are found in PMNT 66/34 compositions, each sintered at 1150,

1200 and 1250°C, respectively (also shown in Table I**).** It can be seen from Figs. 5(i) and 5(ii) that saturated strain% and strain hysteresis% increases with the increase in sintering temperature in PMNT 70/30 and 68/32 compositions and from Fig. 5(iii), saturated strain% increases and strain hysteresis% decreases with the increase in sintering temperature in PMNT 66/34 composition. Generally, the electric field induced strain takes place through micro–domain transformations, domain reorientation and phase transitions [34]. The electric field induced phase transition and domain motion can be accompanied with great hysteresis and high strain [34, 20]. The decrease in saturated strain% and strain hysteresis% in PMNT 70/30 and 68/32 compositions with the decrease in sintering temperature can be explained on the basis of decrease in grain size. In general, the domain wall size decreases with decreasing grain size. And with decreasing grain size, it becomes difficult to form domain walls in the grains and hence the domain rotation contribution to the strain% and strain hysteresis% becomes smaller [33]. Also, the presence of residual stresses in the ceramics prevents domain reversal under external field. And, this effect decreases with the increase in grain size and the decrease in porosity in the ceramic [31]. The increase in saturated strain% with the increase in sintering temperature in PMNT compositions, in MPB region, can be explained on the basis of predominance of electric field induced phase transition and domain wall motion. There can exist mixed structures in PMNT 70/30, 68/32 and 66/34 compositions, since they are in the MPB region [24]. As, can be seen from Fig. 4(i), the presence of two anomalies in ε_r variation with temperature of PMNT 68/32 composition, which indicates about its MPB nature. Also, the hump nature in the plot of ε_r variation with temperature is increasing with the increase in sintering temperature of PMNT 68/32 composition, shown in Fig. 4(i). This gives us hint that with the increase in sintering temperature of PMNT compositions, the mixed phase nature is increasing. And, from Devonshire theory, a little discrepancy of the free energy exists in the mixed structures near MPB of these type of systems. Therefore, domain wall motion and ferroelectric phase transitions are prone to be induced by electric field [35]. Whereas**,** the decrease in strain hysteresis% in PMNT 66/34 compositions with the increase in sintering temperature can be attributed to the increase in engineered domain stability [35].

The piezoelectric coefficient, d_{33}, is calculated from the slope of strain% Vs. electric field (S-E) behavior in the higher field region, using the relation:

$$d_{33} = (\Delta \text{ strain } (\%) / \Delta E) \times 10^6 \text{ pm/V}$$

and d_{33} for different compositions is given in Table II. The development of high d_{33} and high induced saturated strain% ~0.19 with low strain hysteresis% ~3.2 in PMNT 68/32 composition sintered at 1200^{o}C, suggests its suitability for actuator application.

Conclusions

The effect of sintering temperature on the dielectric and strain induced by electric field behaviors of PMNT compositions, in the MPB region, has been studied. ε_r and tanδ increases and Curie transition range decreases with the increase in sintering temperature. The strain levels in the range of 0.07 to 0.2% were obtained. High d_{33} ~320pm/V and saturated strain% ~0.19 with low strain hysteresis% ~3.5 in PMNT 68/32 ceramics sintered at 1200^{o}C indicates its suitability for actuator applications.

References:

1. E. Burcsu, G. Ravichandran and K. Bhattacharya, Appl. Phys. Lett., **77** (2000) 1698.
2. A. A. Bokov and Z.–G. Ye, J. Appl. Phys., **91** (2002) 6656.
3. R. F. Service, Science, **275** (1997) 1878.
4. L. E. Cross: Ferroelectrics **76** (1987) 241.
5. Y.H. Chen, K. Uchino, M. Shen, D. Viehland, J. Appl. Phy., **90** (2001) 1455.
6. G.H. Haertling, J. Am. Ceram. Soc., **82** (1999) 797.
7. S.W. Choi, T.R. Shrout, S.J. Jang , A.S. Bhalla, Ferroelectrics, **100** (1989) 29.
8. J. Kuwata, K. Uchino ans S. Nomura, Ferroelectrics, **37** (1981) 579.
9. J. Kuwata, K. Uchino ans S. Nomura, Jpn. J. Appl. Phys. Part **[2]** (1982) 1298.
10. K. Harada, S. Shimanuki, T. Kobayashi, S. Saitoh and Y. Yamashita, J. Am. Ceram. Soc. **81** (1998) 2785.
11. S. E Park and T. R. Shrout, IEEE Trans. Ultrason. Ferroelectric Freq. Control, **44** (1997) 1140.
12. B. Jaffe, W. Cook and H. Jaffe: *Piezoelectric Ceramics* (Academic Press, London, 1971).
13. P. Kumar, S. Singh, O. P. Thakur, C. Prakash and T. C. Goel, Japanese Journal of Applied Physics, Vol 43, No. 4A, 2004, pp. 1501-1506.
14. T. R. Shrout and A. Halliyal, Am. Ceram. Soc. Bull., **66** (1987) 704.
15. E. A. Young, Y. B. Huang, R. Riddle, Y. Yang and C. Beduz, Physica C: Superconductivity 372-376 (2002) 931.
16. H. R. Rukmini, R. N. P. Choudhary and D. L. Prabhakara: Materials Chemistry and Physics **64** (2000) 171.

17. S. Kang, J. H. Lee, J. J. Kim, H. Y. Lee and S. H. C. Kimura, J. Eur. Ceram. Soc. 24(6), 2004, 1031-1035.
18. T. T. K Hiroshima and T. Kimuru, J. Am. Ceram. Soc., **79** (1996) 3235.
19. Kimura, S. Miyamoto and T. Yamaguchi, J. Am. Ceram. Soc., **73** (1990) 123.
20. Z. Feng, H. Luo, Y. Guo, T. He and H. Xu, Solid State Communications, **126** (2003) 347.
21. S.W. Choi, T.R. Shrout, S.J. Jang , A.S. Bhalla, Mater. Lett., **8** (1989) 253.
22. A. D. Hilton, C. A. Randall, D. J. Barber and T. R. Shrout, Ferroelectrics, **93** (1989) 379.
23. J. Kelly, M. Leonard, C. Tantigate and A. Safari, J. Am. Ceram. Soc., **80** (1997) 379.
24. J. Zhao, Q. M. Zang, N. Kim and T. R. Shrout, Jpn. J. Appl. Phys. Part 1, **34** (1995) 5658.
25. S. L. Swratz, T. R. Shrout, W. A. Schulze and L. E. Cross, J. Am. Ceram. Soc., 67 (1984) 311.
26. J. Chen and M. P. Harmer, J. Am. Ceram. Soc., 73 (1990) 68.
27. H. C. Wang and W. A. Schlze, J. Am. Ceram. Soc. 73 (1990) 825.
28. M. H. Frey, Z. Xu, P. Han and D. A. Payne, Ferroelectrics, 206/207 (1998) 337.
29. F. Xu, R. A. Wolf, T. Yoshimura and S. T. Mckinstry, in Proc. Int. Symp. Electrets (ISE-11), ed. R.J. Flemming (IEEE Inc., Melbourne, 2002), p 386.
30. Z. Surowiak, M. F. Kupriyanov, A. E. Panich and R. Skulski: J. Eur. Ceram. Soc. **21** (2001) 2783.
31. M.E. Lines, A.M. Glass, Principles and Applications of Ferroelectrics and Related Materials, Clarendon Press, Oxford, 1977.
32. K. Furuta and K. Uchino: Advanced Ceramic Materials, **1** (1986) 61.
33. K. Uchino: Ferroelectric Devices (Marcel Dekker, New York, 2000).
34. S. E. Park and T. R. Shrout: J. Appl. Phys., **82** (1997) 1804.
35. D. Vanderbit, M. H. Cohen, Phys. Rev. B, **63** (2001) 094108.

Figure captions:

1. SS50 strain measurement system.

2. XRD patterns of (a) PMNT 70/30, (b) PMNT 68/32 and (c) 66/34 compositions sintered at 1200°C.

3.1 SEM photographs of fractured surfaces of PMNT 70/30 composition sintered at (a) 1150^{o}C, (b) 1200^{o}C and (c) 1250^{o}C.

3.2 SEM photographs of fractured surfaces of PMNT 68/32 compositions sintered at (a) 1150^{o}C, (b) 1200^{o}C and (c) 1250^{o}C.

3.3 SEM photographs of fractured surfaces of PMNT 66/34 composition sintered at (a) 1150^{o}C, (b) 1200^{o}C and (c) 1250^{o}C.

4. Temperature variation of (i) ε_r and (ii) tanδ at 1kHz of PMNT 68/32 composition sintered at (a) 1150, (b) 1200 and (c) 1250°C.

5. Strain% versus unipolar electric field behavior of (i) PMNT 70/30 (ii) PMNT 68/32 and (iii) PMNT 66/34 compositions each sintered at (a) 1150, (b) 1200 and (c) 1250^{o}C.

Table I: Strain hysteresis% in PMNT compositions, in the MPB region, sintered at different temperatures.

Table II: Piezoelectric coeff., d_{33}, from the slope of the (S-E) behavior in the higher electric field region.

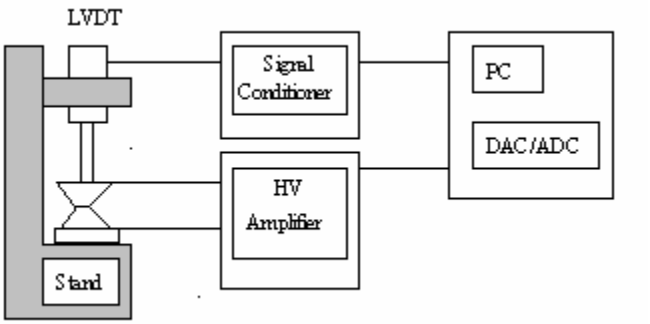

Fig. 1

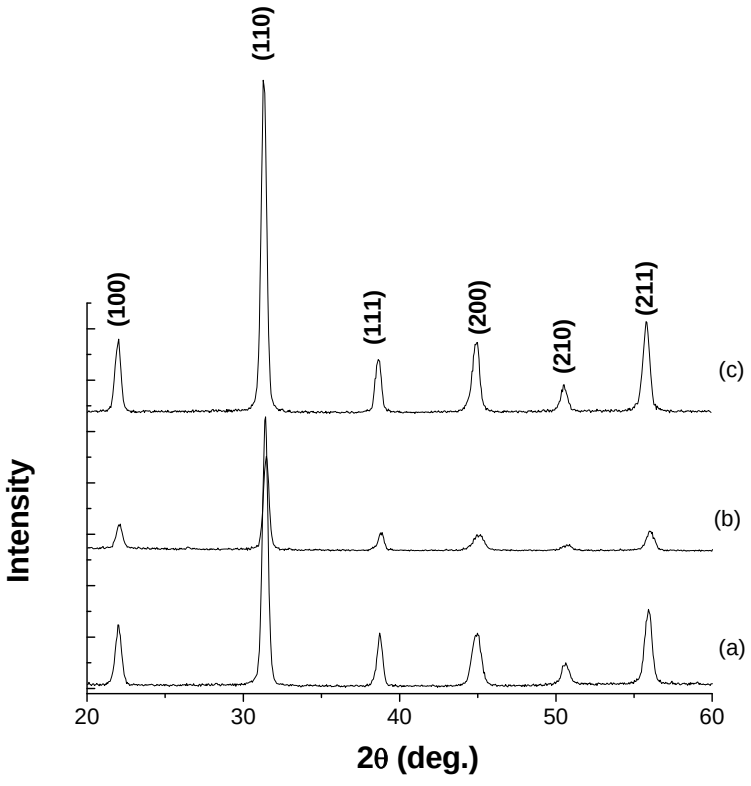

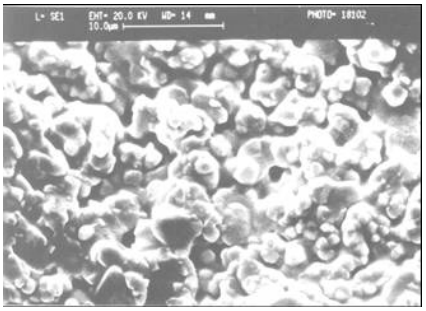

Fig. 2

(a)

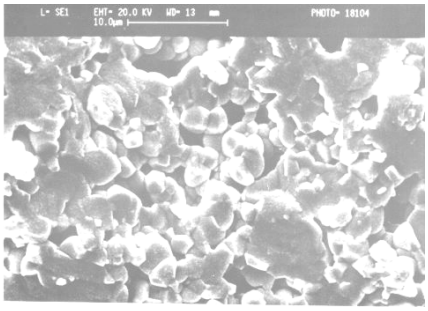

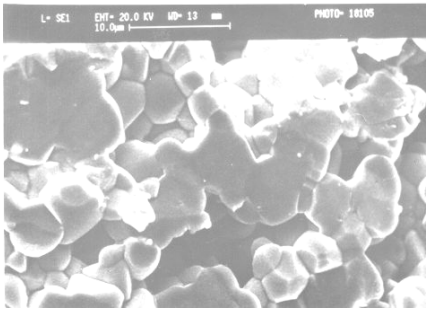

(b) (c)

Fig. 3.1 SEM photographs of fractured surfaces of PMNT 70/30 composition sintered at (a) 1150^{o}C, (b) 1200^{o}C and (c) 1250^{o}C.

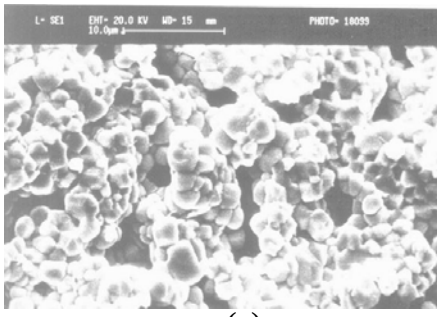

(a)

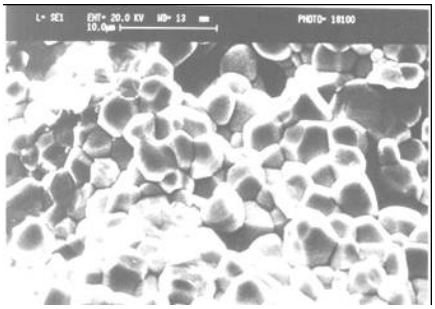

(b)

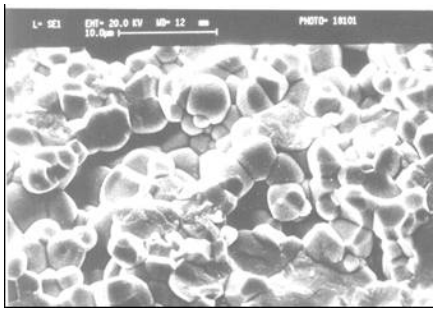

(c)

Fig. 3.2 SEM photographs of fractured surfaces of PMNT 68/32 composition sintered at (a) 1150^{o}C, (b) 1200^{o}C and (c) 1250^{o}C.

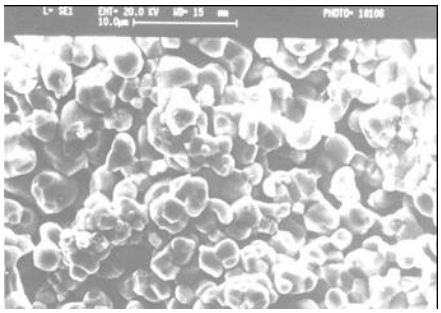

(a)

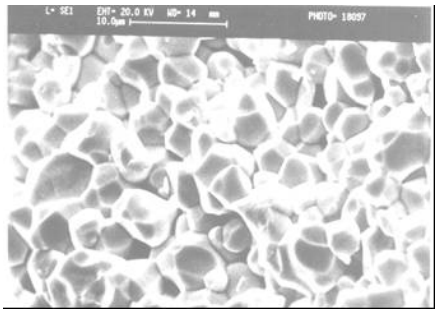

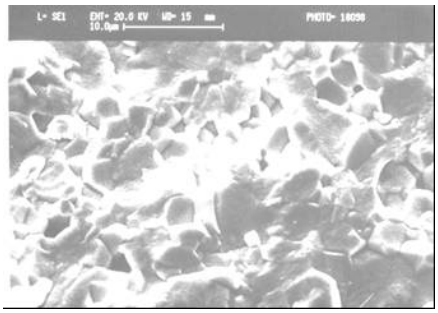

(b) (c)

Fig. 3.3 SEM photographs of fractured surfaces of PMNT 66/34 composition sintered at (a) 1150^{o}C, (b) 1200^{o}C and (c) 1250^{o}C.

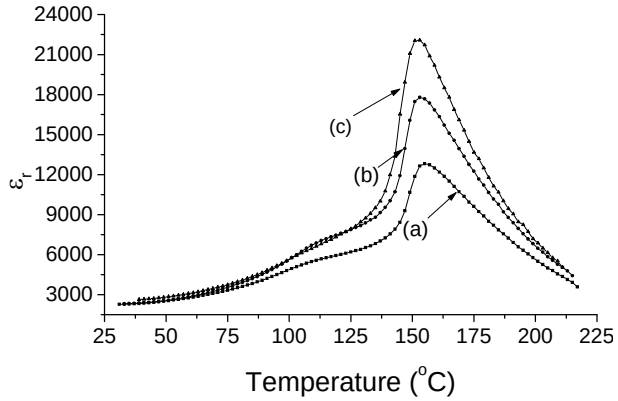

4 (i)

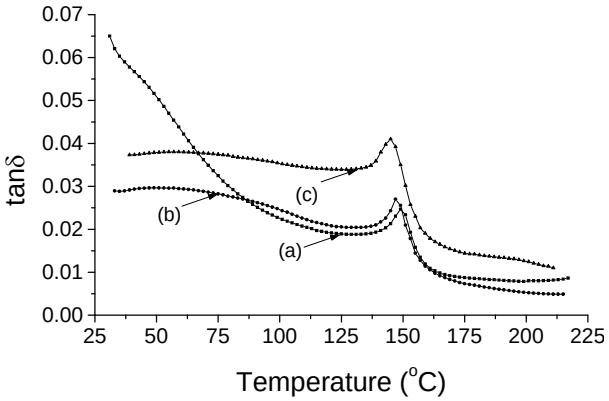

4 (ii)

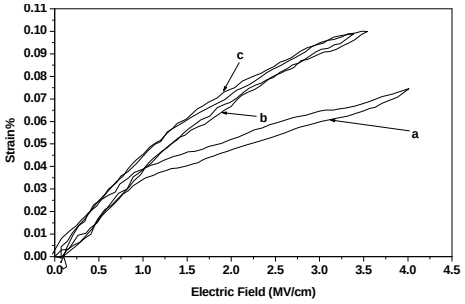

Fig. 5(i)

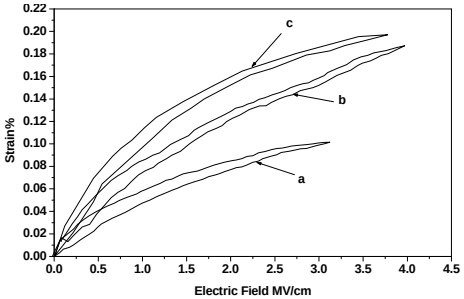

Fig. 5(ii)

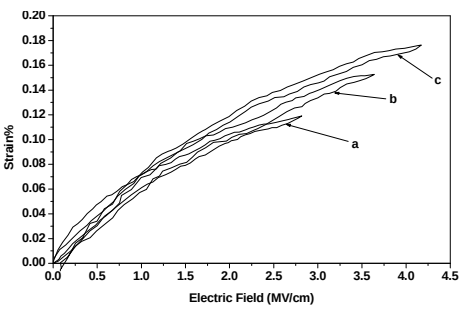

Fig. 5(iii)

Table I

Sintering temperature	Strain Hysteresis%		
	PMNT 70/30	PMNT 68/32	PMNT 66/34
1150°C	6	3.2	6.5
1200°C	6.6	3.5	3.9
1250°C	8.9	6.5	1

Table II

PMNT compositions Sintered at (^{o}C)	70/30 1150	70/30 1200	70/30 1250	68/32 1150	68/32 1200	68/32 1250	66/34 1150	66/34 1200	66/34 1250
d_{33} (pm/V)	205	195	235	130	320	235	190	300	230

List of Changes included in the revised manuscript:

(i) As suggested by the referee, editing of the manuscript throughout the whole text like:
   (i) Grammatical corrections throughout the manuscript.
   (ii) In place of PMNT 66/34 composition, sintered at 1250^{o}C, the PMNT 68/32 composition sintered at 1200^{o}C is suggested as the best material for actuator application.
   (iii) The extra discussion on strain vs. electric field measurement system functioning is excluded.

(ii) As suggested by the referee, the effect of residual porosity on the physical properties of the samples of PMNT system, sintered at three different temperatures.

(iii) As suggested by the referee, Scanning Electron Microscopy (SEM) images of PMNT compositions, sintered at different temperatures, are included.

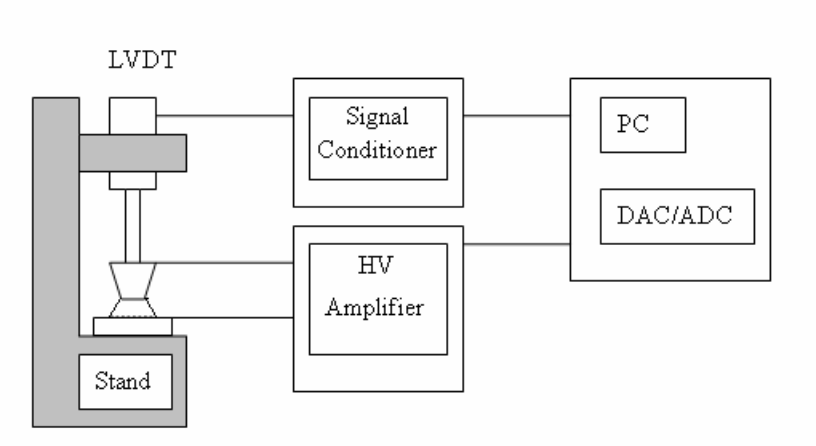
LVDT
Signal Conditioner
PC
DAC/ADC
HV Amplifier
Stand

Fig. 1

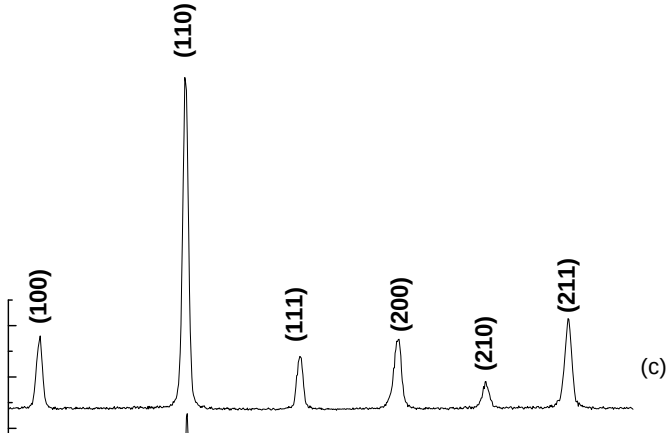
(110)
(100)
(111)
(200)
(210)
(211)
(c)

Fig. 2

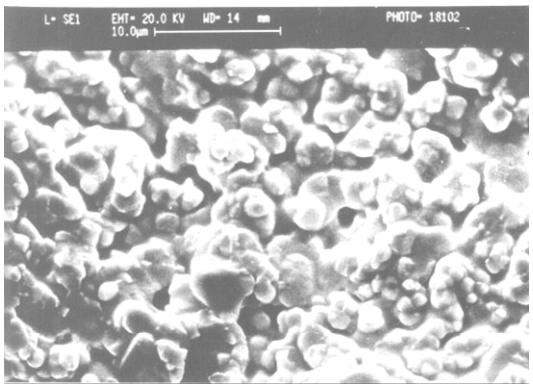
L- SE1 EHT- 20.0 KV WD- 14 mm
10.0µm
PHOTO- 18102

(a)

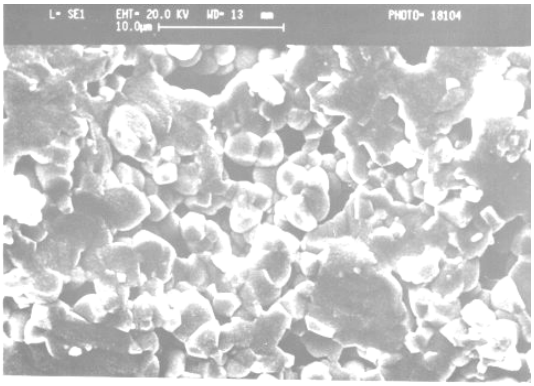
L- SE1 EHT- 20.0 KV WD- 13 mm
10.0µm
PHOTO- 18104

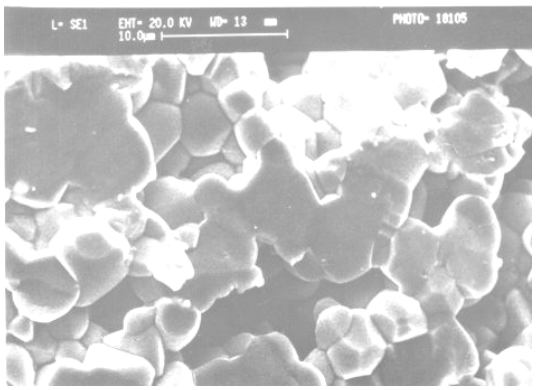
L- SE1 EHT- 20.0 KV WD- 13 mm
10.0µm
PHOTO- 18105

(b) (c)

Fig. 3.1 SEM photographs of fractured surfaces of PMNT 70/30 composition sintered at (a) 1150^{o}C, (b) 1200^{o}C and (c) 1250^{o}C.

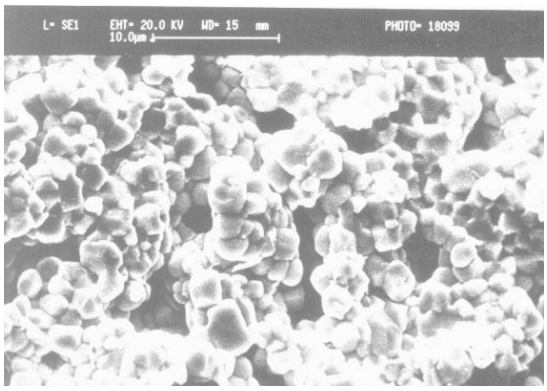

(a)

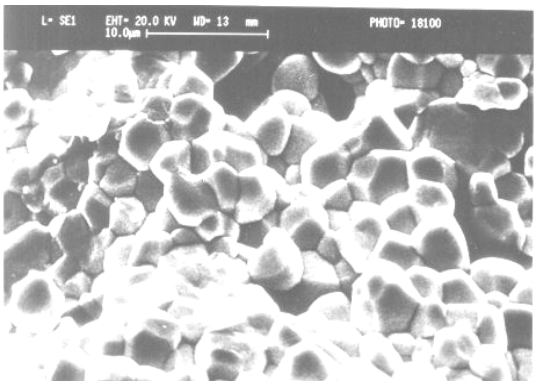

(b)

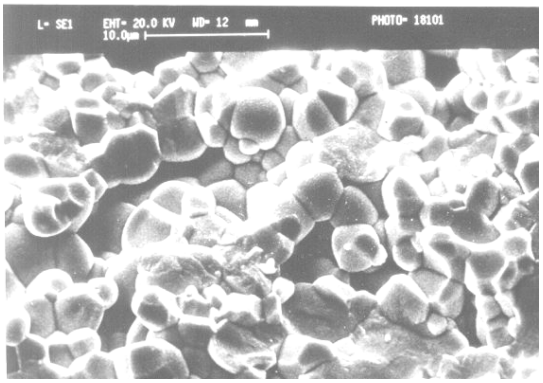

(c)

Fig. 3.2 SEM photographs of fractured surfaces of PMNT 68/32 composition sintered at (a) 1150^{o}C, (b) 1200^{o}C and (c) 1250^{o}C.

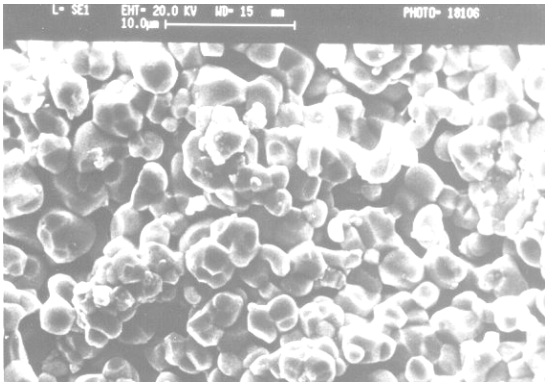

(a)

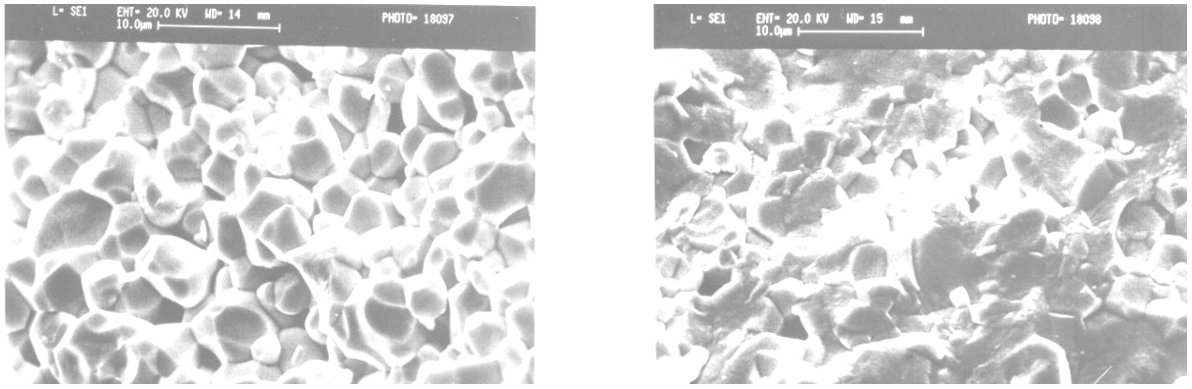

(b) (c)

Fig. 3.3 SEM photographs of fractured surfaces of PMNT 66/34 composition sintered at (a) 1150^{o}C, (b) 1200^{o}C and (c) 1250^{o}C.

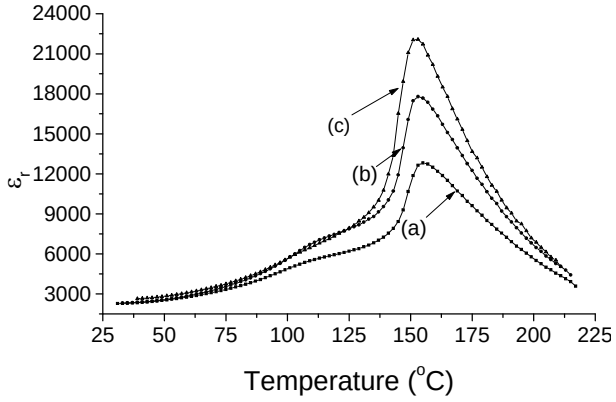

4 (i)

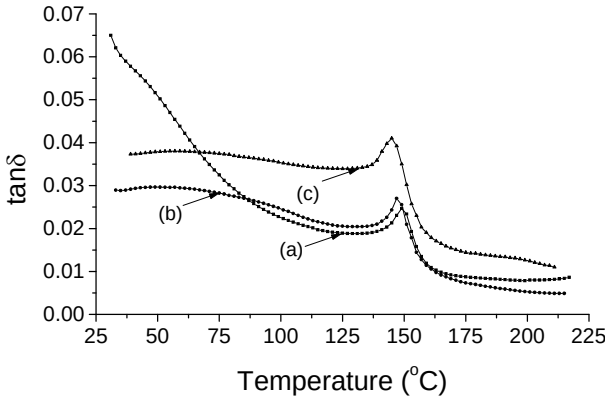

4 (ii)

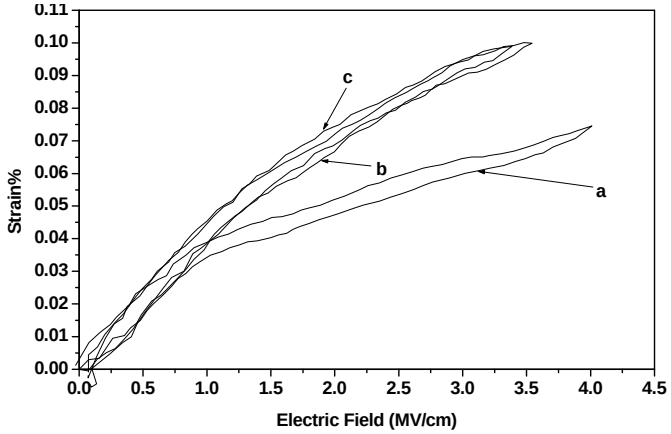

Fig. 5(i)

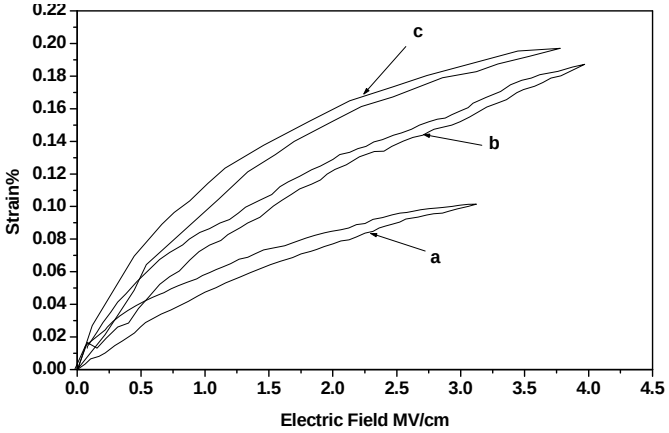

Fig. 5(ii)

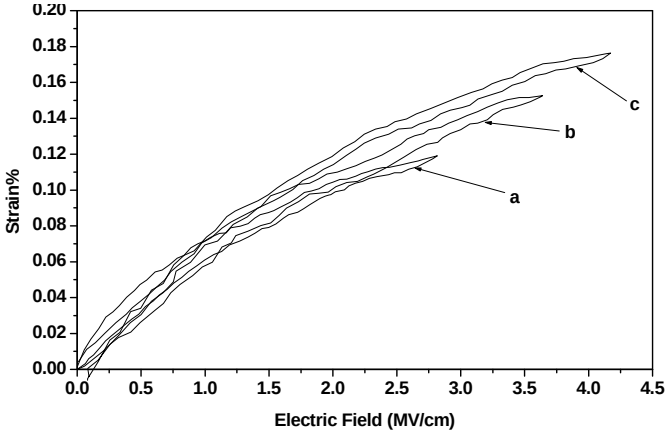

Fig. 5(iii)